INTERNATIONAL JOURNAL FOR NUMERICAL METHODS IN FLUIDS, VOL. 25, 547–566 (1997)

MULTIDOMAIN IMPLICIT NUMERICAL SCHEME

A. POVITSKY* AND M. WOLFSHTEIN

Faculty of Aerospace Engineering, Technion—Israel Institute of Technology, Technion City, Haifa 3200, Israel

SUMMARY

A multidomain method for the solution of elliptic CFD problems with an ADI scheme is described. Two methods of treatment of internal boundary conditions for ADI functions are discussed, namely an explicit and a semi-implicit method. Stability conditions for the proposed methods are derived theoretically. The semi-implicit scheme is more stable than the explicit scheme, leading to improved numerical efficiency for multidomain computations. Numerical computations for a linear convection–diffusion equation, for buoyancy-driven recirculating flow in a square cavity and for turbulent flow in a square duct confirmed the theoretical results. Computer runs of the multidomain code in a distributed memory multiprocessor system were successful and efficient and produced reliable results. © 1997 by John Wiley & Sons, Ltd.

Int. J. Numer. Meth. Fluids, **25**: 547–566 (1997).

No. of Figures: 7. No. of Tables: 4. No. of References: 21.

KEY WORDS: parallel computing; implicit scheme; multidomain computations; stability; turbulent flow; duct flow

1. INTRODUCTION

The development of multidomain schemes is important for parallel computing on distributed memory machines, for problems with complicated geometry and for the reduction of round-off errors on fine grids.[1]

Explicit schemes are easy to implement in multidomain applications. However, such schemes suffer from a short time step owing to stability limitation. Implicit schemes have less restrictive stability limitations. For instance, the two-dimensional ADI scheme considered in this paper is absolutely stable for a linear equation. On the other hand, implicit schemes are characterized by global spatial data, dependences and a requirement to solve large-bandwidth linear systems. In the present work some ways to apply multidomain techniques to the Douglas alternating direction implicit (ADI) scheme are studied. In an implicit scheme it is usually required to solve a linearized system of equations for every time step. The coefficient matrix of this system is usually pentadiagonal and very large. In the ADI method this large matrix is split into many tridiagonal matrices which are much easier to solve. However, the standard tridiagonal solver is recursive. Therefore it is difficult to implement the algorithm for tridiagonal matrices which are artificially split owing to the need to solve the problem over subdomains. This problem is resolved by algorithmic changes reducing spatial data dependences and 'far-field' interaction between subdomains. These changes may cause certain

*Correspondence to: A. Povitsky, Faculty of Aerospace Engineering, Technion—Israel Institute of Technology, Technion City, Haifa 3200, Israel.

CCC 0271–2091/97/050547–20 $17.50

Received January 1996
Revised November 1996

degradation of the numerical efficiency and in some cases even loss of stability. In this paper we examine some possible methods to define artificial boundary conditions at subdomain interfaces and the influence of these methods on the stability and numerical efficiency of the proposed schemes. The problem of parallelization of such schemes and the loss of efficiency due to communication between processors are discussed elsewhere.[2]

1.1. Literature Survey

Various authors have studied the parallelization of ADI schemes. For instance, Naik *et al*.[3] used the Beam–Warming ADI scheme to solve the 3D Euler and thin layer equations in the frame of a multidomain approach. They overcame the recursiveness of the Thomas algorithm for the solution of tridiagonal systems of equations by sending the necessary information (the coefficients of the Thomas algorithm on the forward step and the values of the solution vector on the backward step) to neighbouring subdomains after every line or row of the ADI sweeps. This procedure, referred to as the 'pipeline Thomas algorithm', does not need any internal interfacial boundary conditions. However, this leads to a penalty when the method is parallelized, as each processor has to wait for all the processors behind it (in the first step of the Thomas algorithm) and for all the processors ahead of it (in the second step of the Thomas algorithm) before the next iteration can start.

Rosenfeld and Yassour[4] define different sets of subdomains for each stage of the ADI method. Each subdomain stretches between two physical boundaries of the problem. This eliminates the need for specific non-physical boundary conditions at the subdomain interfaces with the accompanying numerical difficulties. However, this method is unsuitable for distributed memory machines owing to the necessity to exchange the computational matrices between processors at each stage of an ADI method.

A very common approach to the problem of semi-implicit or implicit multidomain solution methods is to compute the internal boundary values explicitly as was done by Schreck and Peric,[5] who used subdomain partitioning in a SIMPLE-based Navier–Stokes solver. They parallelized the SIMPLER solver by straightforward utilization of internal boundary values for the governing variables from the previous iteration. Internal boundary values of the governing variables were exchanged after each sweep. This approach was used also by Tsai[6].

Although such an approach appears suitable for a semi-implicit scheme such as SIMPLE, Braten[7] has shown that the convergence rate of this method deteriorates in comparison with its single-domain version, because internal boundary values for the governing variables are updated explicitly. According to Braten, any improvement in the convergence rate obtained by increasing the number of internal sweeps is more than offset by the longer time requirement per iteration.

A somewhat different approach was used by Jenssen,[8] who carried out implicit multiblock computations for a large number of blocks using explicit coupling between the blocks. This method is very sensitive to the block partitioning. Jenssen computed a spectral radius for the characteristic matrix for the one-dimensional scalar linear convection–diffusion equation with constant coefficients for a two-level upwind scheme. In the multiblock case the spectral radius is close to unity for a mesh Reynolds number less than one. It was concluded theoretically and by computer runs that the Navier–Stokes equations are not decoupled in regions with strong parabolic dominance such as boundary layers.

Degani and Marcus[9] proposed improving the stability of domain decomposition schemes by a choice of an optimal number of overlapping grid points in the frame of an explicit approach to the internal boundary values. They obtained (by computer experiments) the critical Courant number for the inception of instability as a function of the number of overlapping segments for the MacCormack explicit and Beam–Warming implicit methods applied to the Euler equations.

Tysinger and Caughey[10] used an ADI scheme to solve the Navier–Stokes equations for viscous compressible subsonic flow on a distributed system of IBM RISC workstations. The boundary values on subdomain interfaces were treated in a manner consistent with the theory of characteristics. No interblock communication is required for such a treatment. Convergence rates were nearly the same for the single- and multidomain schemes. However, only five subdomains were used in this research. The authors comment that in general it is possible to construct implicit interface boundaries, but further communications and synchronization costs would be incurred.

Thus it appears that an estimation of the internal boundary conditions on subdomain boundaries is the critical step for the implementation of implicit numerical schemes for multidomain computations.

1.2. Purpose and scope of present contribution

The aim of this work is to find an effective method for the determination of artificial boundary values on the internal interfacial boundaries between the subdomains for the Douglas ADI method with a second-order finite difference scheme. The algorithm proposed here differs from that of Naik *et al.*[3] in that the calculations in each subdomain must wait for their neighbours only and need not wait for completion of each step of the solution in all subdomains. A single-point overlap is used in order to minimize the communication and computation penalty for parallel implementation.

In the present paper we attempt to preserve the stability features of the basic single-block implicit scheme. A theoretical prediction of the stability of multidomain schemes for the convection–diffusion equations is derived and tested numerically.

2. MATHEMATICAL FORMULATION

Consider a partial differential equation of the form

$$\frac{\partial \phi}{\partial t} = L\phi + S, \tag{1}$$

where t is the time, $L = A_x + A_y$ is a two-dimensional elliptic differential operator and S is a source term.

The Douglas ADI method (sometimes referred to as the Samarskii–Andreev method) is used here following Isenberg and de Vahl Davis:[11]

$$\left(I - \frac{\Delta t}{2} A_x\right) f^* = (A_x + A_y)\phi^n + S^n, \tag{2}$$

$$\left(I - \frac{\Delta t}{2} A_y\right) f^{**} = f^*, \tag{3}$$

$$\phi^{n+1} = \phi^n + \Delta t f^{**}. \tag{4}$$

The boundary condition for the auxiliary functions f^* and f^{**} is easily obtained from the above definition. In particular, in a steady state these boundary values are equal to zero.

3. MULTIDOMAIN SCHEME

3.1. Domain partitioning

In the current work a rectangular domain was divided regularly into rectangular subdomains. Thus each subdomain has a maximum of two neighbours for a one-dimensional partitioning and four

neighbours for a two-dimensional partitioning. A single-boundary-point overlap is used on all internal domain boundaries (see Figure 1). For instance, the points in the Nth column in Figure 1 are internal points of the first subdomain. The points in the $(N+1)$th column are boundary points of the first subdomain. In turn, points belonging to the $(N+1)$th column are internal points of the second subdomain and points belonging to the Nth column are boundary points of the second subdomain. Thus the first point in a given domain is also the boundary point in the previous domain (except for the points on the physical boundaries). After each time step the values of the governing variables and velocities on subdomain interfaces are exchanged between subdomains. Additionally one should specify the internal boundary conditions for the ADI functions. A fully explicit and a semiimplicit approximation of the internal boundary conditions for the ADI functions are described below.

3.2. *Fully explicit scheme*

For all internal boundaries the auxiliary functions at the $(i+1)$th step were taken from the values of the governing variables at the two previous steps:

$$f_{\mathrm{b}}^{*i+1} = R(\phi_{\mathrm{b}}^{i} - \phi_{\mathrm{b}}^{i-1})/\Delta t, \tag{5}$$

where $0 \leqslant R \leqslant 1$ is a damping coefficient. In the fully explicit scheme the boundary values of the auxiliary ADI functions are not exchanged between subdomains.

3.3. *Semi-implicit scheme*

The internal boundary values of the auxiliary functions at the front of the subdomain (relative to the direction of integration) were obtained by the fully explicit scheme described above. The internal boundary values at the back were obtained from the ADI solution for the previous domain at the same time step. When this scheme is incorporated in a parallel solver, these internal boundary values are transferred from the processor corresponding to the previous domain via the communication network. The scheme is called 'semi-implicit' because the values at the back of the subdomain are calculated at the $(i+1)$th step by the implicit ADI method. The main advantage of the semi-implicit scheme is its improved stability (see below). Its drawback for parallel computer application is additional

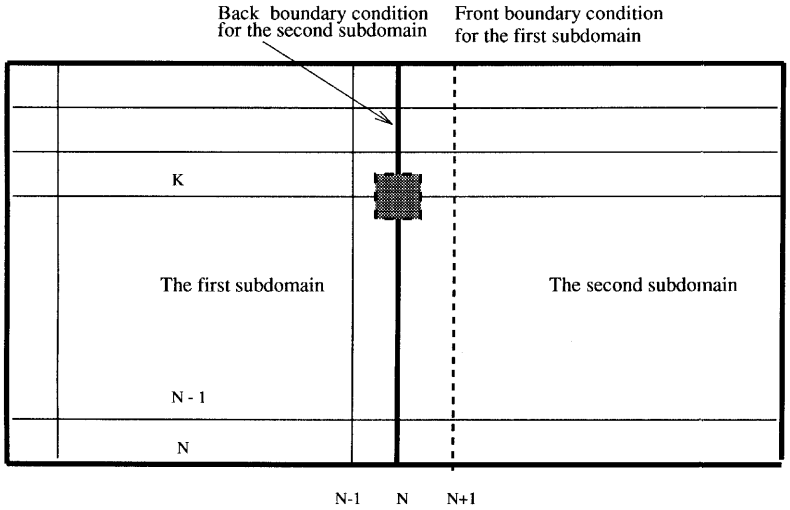

Figure 1. Subdomains overlap

communication between processors and processor idle time, because the boundary values of the auxiliary ADI functions are required for computations in the subdomain ahead of the current subdomain.

4. STABILITY ANALYSIS

The von Neumann stability analysis is used here. The application of the method to internal points is well known. However, we recapitulate it here as a starting point for its extension to the treatment of the internal boundaries.

4.1. Internal points

For a two-dimensional scalar transport equation the operators A_x and A_y of the ADI equations are written in the second-order non-staggered finite difference form

$$A_x\phi^n = \Delta t^{-1}\left(S_x(\phi^n_{N-1,M} - 2\phi^n_{N,M} + \phi^n_{N+1,M}) - \frac{C_x}{2}(\phi^n_{N+1,M} - \phi^n_{N-1,M})\right), \tag{6}$$

$$A_y\phi^n = \Delta t^{-1}\left(S_y(\phi^n_{N,M-1} - 2\phi^n_{N,M} + \phi^n_{N,M+1}) - \frac{C_y}{2}(\phi^n_{N,M+1} - \phi^n_{N,M-1})\right), \tag{7}$$

where

$$S_x = \nu\Delta t/\Delta x^2, \qquad S_y = \nu\Delta t/\Delta y^2, \qquad C_x = U\Delta t/\Delta x, \qquad C_y = V\Delta t/\Delta y. \tag{8}$$

It may be noted that C is the Courant number and S (often referred to as the 'stability ratio') is indicative of the stability of parabolic systems. C/S is the cell Reynolds number.

The error is defined as the difference between the exact and the numerical solution:

$$\varepsilon_n = \phi_{\text{exact}} - \phi^n. \tag{9}$$

The variable ϕ_{exact} satisfies the PDEs. As the equations are linearized about the exact solution, the finite difference equations govern ε as well, but with zero boundary conditions. Therefore the error ε (around the known solution) and the ADI functions for the error, f^* and f^{**}, may be expanded into Fourier series as

$$\varepsilon = G^n e^{(\theta_x N + \theta_y M)\mathrm{i}}, \tag{10}$$

$$f^* = P e^{(\theta_x N + \theta_y M)\mathrm{i},} \tag{11}$$

$$f^{**} = Q e^{(\theta_x N + \theta_y M)\mathrm{i}}, \tag{12}$$

where G, P and Q are amplification factors, N and M are the numbers of mesh points in the x- and y-direction respectively and θ_x and θ_y are the phases, which are the same for both the ADI functions and the error. It is now possible to substitute these definitions in the finite difference expressions for $A_x\phi$ and $A_y\phi$ in the ADI formulae (2) and (3) to get equations for the amplification factors P, Q and G:

$$(1 + X/2)P = -\Delta t^{-1}(X + Y)G^n, \tag{13}$$

$$(1 + Y/2)Q = P, \tag{14}$$

$$G^{n+1} = G^n + Q\Delta t, \tag{15}$$

where

$$X = 4S_x \sin^2\left(\frac{\theta_x}{2}\right) + C_x \sin(\theta_x)\mathrm{i}, \qquad Y = 4S_y \sin^2\left(\frac{\theta_y}{2}\right) + C_y \sin(\theta_y)\mathrm{i}. \tag{16}$$

The final expression for the amplification factor G is

$$G = 1 - \frac{X + Y}{(1 + X/2)(1 + Y/2)}. \tag{17}$$

The absolute stability condition is $|G| > 1$ for every X and Y. It is possible to show[12] that this condition is satisfied and the scheme is unconditionally stable for S_x, $S_y \neq 0$. It should be noted that this proof is for a single linear equation and not for the non-linear system of the Navier–Stokes equations.

4.2. Explicit scheme

The stability analysis for the internal boundaries follows that of Trapp and Ramshaw,[13] who employed a similar technique for the real boundaries of their computational domain. The analysis is based on the von Neumann analysis of the finite difference equations in the neighbourhood of the internal boundary points, A local stability analysis at a given mesh point is performed by estimating the amplification factor from the relation between the values of the error at the neighbouring mesh points to which the given point is directly coupled by the finite difference scheme.[13] The obtained expressions for the amplification factor are valid for all A_x and A_y. The detailed numerical computations of the stability region will be performed for the case $A_x = A_y$ (corresponding to $S_x = S_y$ and $C_x = C_y$). Further, the stability regions for different A_y will be computed. The partial case $A_y = 0$ will be considered for one-dimensional applications.

To illustrate the method, we consider an internal boundary perpendicular to the x-direction. The RHS of the first ADI equation becomes

$$\left(I - \frac{\Delta t}{2}A_x\right)f^* = P\left[1 + S_x - \left(\frac{S_x}{2} + \frac{C_x}{4}\right)\mathrm{e}^{-\theta_x \mathrm{i}}\right] + \Delta t^{-1}\left(\frac{C_x}{4} - \frac{S_x}{2}\right)G^{n-1}R(G-1)\mathrm{e}^{\theta_x \mathrm{i}}. \tag{18}$$

Substitution of this expression into the first ADI equation (2) leads to a quadratic equation for the amplification factor G:

$$AG^2 + BG + C = 0, \tag{19}$$

where

$$A = \left(1 + \frac{Y}{2}\right)\left[1 + S_x - \left(\frac{S_x}{2} + \frac{C_x}{4}\right)\mathrm{e}^{-\theta_x \mathrm{i}}\right],$$

$$B = -\left\{\left(1 + \frac{Y}{2}\right)\left[1 + S_x - \left(\frac{S_x}{2} + \frac{C_x}{4}\right)\mathrm{e}^{-\theta_x \mathrm{i}}\right] - \left[X + Y + R\left(\frac{C_x}{4} - \frac{S_x}{2}\right)\mathrm{e}^{\theta_x \mathrm{i}}\right]\right\}, \tag{20}$$

$$C = -R\left(\frac{C_x}{4} - \frac{S_x}{2}\right)\mathrm{e}^{\theta_x \mathrm{i}}.$$

In a similar way it is possible to formulate the quadratic equation for the amplification factor for an internal boundary perpendicular to the y-direction. The resulting equation (19) with coefficients (20) should be solved for G in order to find the condition $|G| < 1$. This was done numerically and the results are shown in Figure 2, where the boundaries of the stability region are depicted in a cell

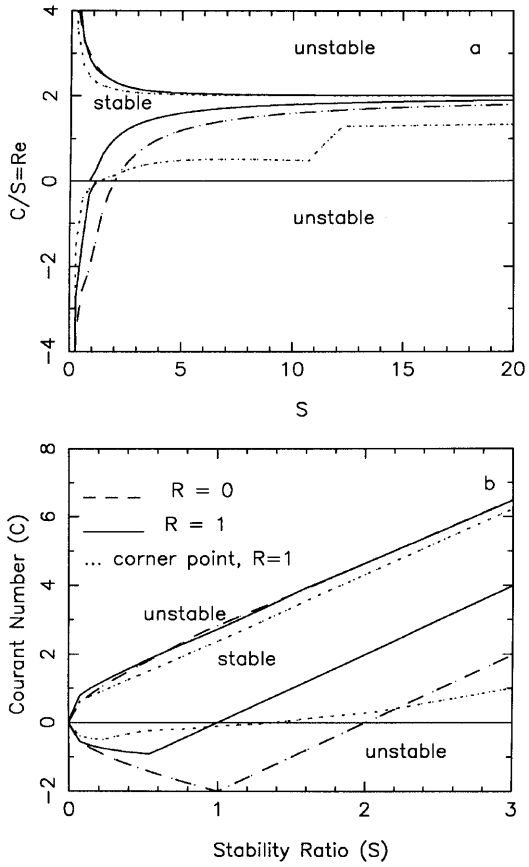

Figure 2. Stability region for explicit scheme: a, large S-values in C/S versus S plane; b, small and moderate S-values in C versus S plane

Reynolds number $Re = C/S$ versus S plane for large S in Figure 2a and in a C versus S plane for small S in Figure 2b. The computations were performed for $A_x = A_y$. The stability region is found between these boundaries. The influence of the operator A_y on the stability region for an internal boundary perpendicular to the x-direction is presented in Figure 3a. It may be concluded that this influence is minor. To complete the picture, we explored the stability limits for very high S. This can be done analytically (see Appendix I). The results show that the condition $|G| \leqslant 1$ is satisfied only for $Re = 2$. Thus a nearly symmetrical (about $Re = 2$) stability region is obtained, asymptotically narrowing towards an infinite S.

The coefficients of the quadratic equation for the amplification factor for corner points are presented in Appendix I. The stability of corner points is shown in Figure 2 and it does not alter the stability region considerably.

4.3. Semi-implicit scheme

For the semi-implicit scheme (an internal boundary perpendicular to the x-direction is considered) two amplification factors for the ADI function f^* should be considered, namely P_1 for the last point of the current subdomain and P_2 for the first point of the next subdomain.

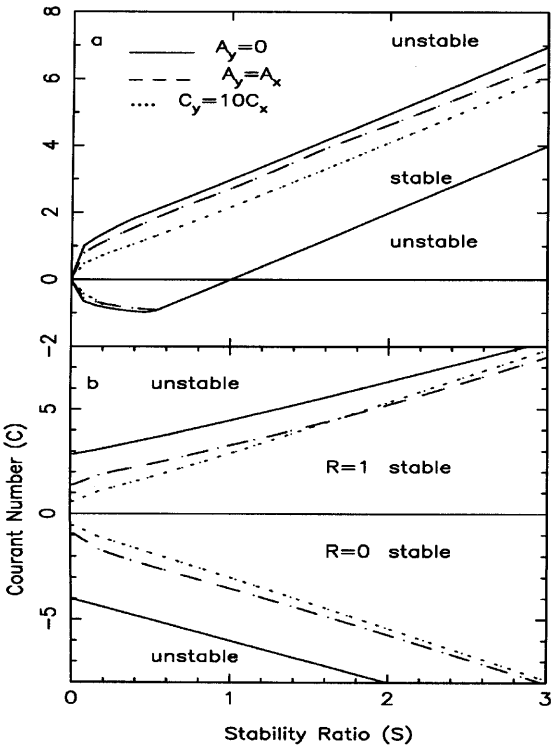

Figure 3. Stability regions for various operators A_y: a, explicit scheme; b, semi-implicit scheme

Commonly in this case the amplification factors for the two sides of the boundary differ. In order to check the stability of the scheme, we assume that the error function ε is represented by a Fourier series

$$\varepsilon = G(n)\mathrm{e}^{(\theta_x N+\theta_y M)\mathrm{i}}, \tag{21}$$

where n is the number of the time step and $G(n)$ is equal to $G_1(n)$ for the explicit (rear) side of the boundary and $G_2(n)$ for the implicit (front) side of the boundary. The factors P_1 and P_2 are computed as

$$P_1 = -\Delta t^{-1}\frac{\left[(X+Y)G_1(n)+R\left(-\frac{S_x}{2}+\frac{C_x}{4}\right)\mathrm{e}^{\theta_x\mathrm{i}}\right]-\left(S_x-\frac{C_x}{2}\right)[G_2(n)-G_1(n)]\mathrm{e}^{\theta_x\mathrm{i}}}{1+S_x-\left(\frac{S_x}{2}+\frac{C_x}{4}\right)\mathrm{e}^{-\theta_x\mathrm{i}}}, \tag{22}$$

$$P_2 = -\Delta t^{-1}\frac{\left[(X+Y)G_2(n)+P_1\left(\frac{S_x}{2}+\frac{C_x}{4}\right)\mathrm{e}^{-\theta_x\mathrm{i}}\right]-\left(S_x+\frac{C_x}{2}\right)[G_2(n)-G_1(n)]\mathrm{e}^{-\theta_x\mathrm{i}}}{1+S_x-\left(\frac{S_x}{2}-\frac{C_x}{4}\right)\mathrm{e}^{\theta_x\mathrm{i}}}. \tag{23}$$

The next-step values of the functions G_1 and G_2 are calculated by the expressions

$$G_{1,2}(n+1) = G_{1,2}(n) + \frac{P_{1,2}}{(1+Y/2)\Delta t}. \tag{24}$$

Results of numerical parametric computations (22)–(24) for G_1 and G_2 are shown in Figure 4 for the one-dimensional case ($A_y = 0$). Computational parameters are presented in the Table I.

The initial amplification factors $G_1(1)$ and $G_2(1)$ are complex numbers with $|G_1(1)| = |G_2(1)| = 1$ and alternating phase angle. Numerical calculations show that the functions G_1 and G_2 approach each other after a large number of iterations. This number of iterations depends on the sign and value of Re, the stability ratio S and the damping coefficient R. Therefore it is possible to analyse the scheme under the assumption $G_1 \approx G_2 \approx G^n$. The analysis follows a pattern very similar to that of the previous subsection. The coefficients of the resulting quadratic equation for the amplification factor G at the internal boundary are

$$A = \left(1+\frac{Y}{2}\right)\left[1+S_x-\left(\frac{S_x}{2}+\frac{C_x}{4}\right)e^{-\theta_x i}\right]\left[1+S_x-\left(\frac{S_x}{2}-\frac{C_x}{4}\right)e^{\theta_x i}\right],$$
$$C = -R\left(\frac{C_x}{4}-\frac{S_x}{2}\right)\left(\frac{S_x}{2}+\frac{C_x}{4}\right), \qquad B = X+Y-(A+C). \tag{25}$$

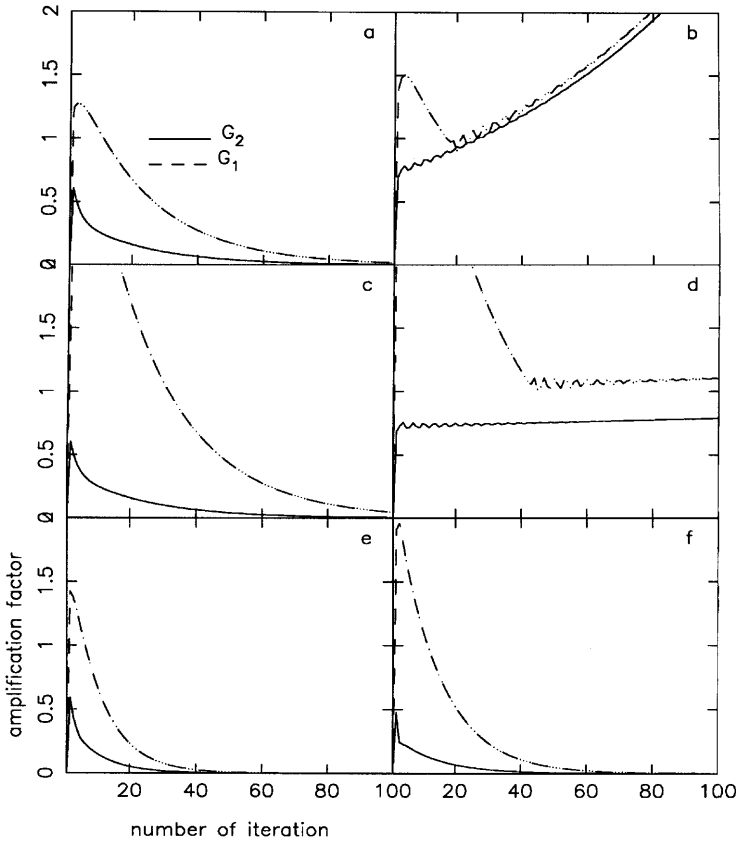

Figure 4. Amplification factors versus number of iterations for semi-implicit scheme

Table I. Parameters for computation of amplification factors $G_{1,2}$

Case	Re	Stability ratio S	Damping coefficient R	Convergence
a	1	10	0	+
b	1	10	0·4	−
c	−1	10	0	+
d	−1	10	0·4	−
e	0	5	0	+
f	0	5	1	+

The quadratic equation was solved numerically to give complex values of the amplification factor. The boundaries of the regions of stability are shown in Figure 5 in the C/S versus S plane. The coefficients (25) of the quadratic equation (19) for the amplification factor are symmetrical relative to C. Therefore the stability regions are presented only for positive C-values. Figure 5a depicts the stability region for large S, while Figure 5b enlarges the small-S region. It may be seen that the scheme is stable ($G \to 0$ for large n) for cell Reynolds numbers $|Re| = 2$ and $Re = 0$ regardless of the stability ratio S and the damping coefficient R. This is confirmed by previous computations of $G_{1,2}$

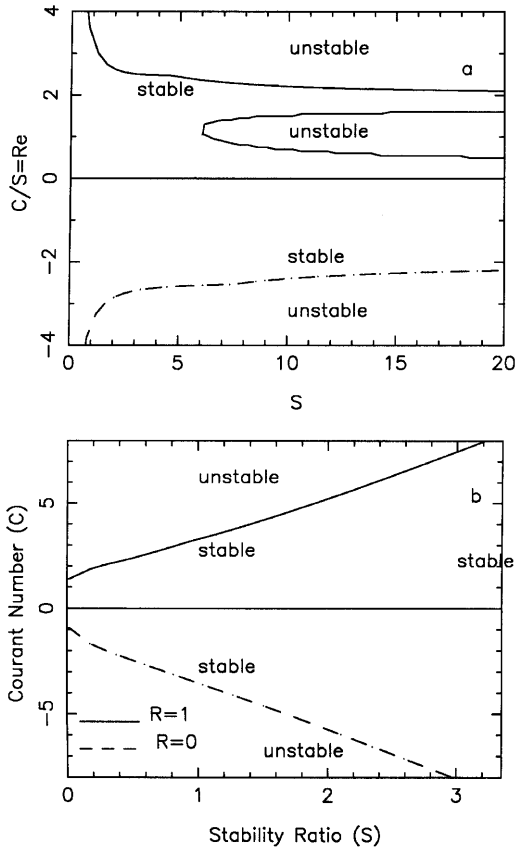

Figure 5. Stability region for semi-implicit scheme: a, large S-values in C/S versus S plane; b, small-values S in C versus S plane

(see Figures 4e and 4f). For $S > 6$ and $R = 1$ an inner unstable region appears inside the stable region. Still the stability region is broader than in the explicit case for all values of S (compare Figures 2 and 5). Fortunately, for $R = 0$ the semi-implicit scheme is stable for all $|Re| \leqslant 2$ regardless of S. The same results are obtained by computations of $G_{1,2}$ for $|Re| = 1$ and $S = 10$ (see Figures 4a and 4d).

For $s \to 0$ the limiting C-value tends to some finite positive number that depends on the damping coefficient and the operator A_y (see Figure 3b). However for the explicit scheme this limiting C-value tends to zero (see Figures 2b, 3a and 7). The influence of the operator A_y on the stability properties of the semi-implicit scheme is presented in Figure 3b. Again, as in the explicit case, this influence is not very noticeable. An analytical investigation of the stability for small and large S is given in Appendix II.

The advantages of the semi-implicit scheme over the explicit scheme can be summarized as follows: (i) the stability condition is symmetrical for positive and negative C-values; (ii) the region of stability is sufficiently larger; (iii) for $R = 0$ and $S_x \to \infty$ the scheme is stable for $|C_x/S_x| \leqslant 2$; (iv) for $S_x \to 0$ the scheme is conditionally stable.

The disadvantages of the semi-implicit scheme for implementation on parallel computers are additional communication time for transfer of the boundary values of the auxiliary ADI functions and local dependence delay of processors.

5. NUMERICAL SOLUTION OF THE SAMPLE PROBLEMS

5.1. One-dimensional convection–diffusion equation

A linear 1D convection–diffusion equation is examined as an example for our stability considerations in the case $A_y = 0$:

$$\frac{\partial U}{\partial t} = -a\frac{\partial U}{\partial x} + \nu\frac{\partial^2 U}{\partial x^2}, \tag{26}$$

with boundary conditions $U(0) = 0$, $U(1) = 1$ and constant a.

This equation has the analytical solution[12]

$$U(x) = \frac{\exp(ax/\nu) - 1}{\exp(a/\nu) - 1}. \tag{27}$$

The computer runs were performed for a stability ratio $S = 20$ and Reynolds numbers $Re = 0{\cdot}1$, 1 and 2. The internal boundary is located at $x = 0{\cdot}8$ (the point of maximal discrepancy between the numerical and analytical solutions for the single-domain case). The semi-implicit scheme is utilized for boundary values of the ADI function. The numerical errors versus the number of iterations are shown for the single-domain case (full lines in Figure 6) and for the two-domain computations with internal boundary (broken lines in Figure 6).

The instability of the fully explicit scheme (Section 3.2) is shown in Figure 6 (curve 4), where the error is drastically increased. The semi-implicit scheme is stable everywhere in this set of computations. The rate of decrease of the discrepancy is close to that of the single-domain case. For the specific case $Re = 2$ the convergence graphs nearly coincide. Even for a case of instability of the internal boundary ($|Re| = 1$, $R = 1$) the computations are stable as a result of the stability of the internal points.

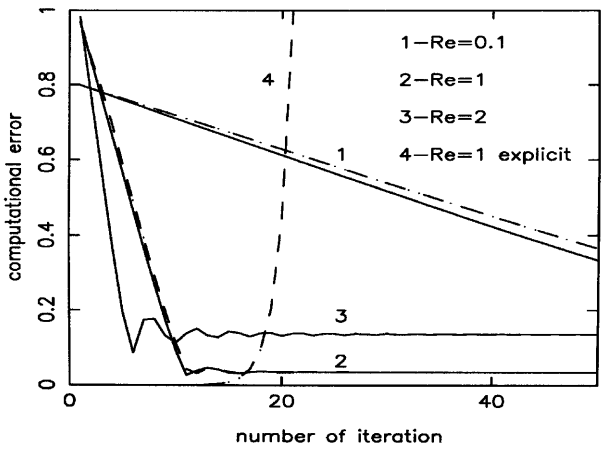

Figure 6. Convergence history for linear convection–diffusion equation: full lines, serial case; broken lines, computations with internal boundary

5.2. *Buoyancy-driven flow in a square cavity*

The problem is as follows. The horizontal walls are adiabatic and the vertical walls are at non-dimensional temperatures of zero and one. The Boussinesq approximation for buoyancy forces is used. The governing equations in non-dimensional form are:

$$\frac{\partial(U\xi)}{\partial x}+\frac{\partial(V\xi)}{\partial y}=Pr\nabla^2\xi+RaPr\frac{\partial T}{\partial x}, \tag{28}$$

$$\frac{\partial(UT)}{\partial x}+\frac{\partial(VT)}{\partial y}=Pr\nabla^2 T, \tag{29}$$

$$0=\nabla^2\psi+\xi, \tag{30}$$

$$U=\frac{\partial\psi}{\partial y}, \qquad V=-\frac{\partial\psi}{\partial x}. \tag{31}$$

No-slip impermeable solid walls are assumed. Boundary conditions for the vorticity at the walls were approximated by the Woods second-order formula[14]

$$\xi_{\mathrm{B}}=\frac{3(\psi_{\mathrm{B+}}-\psi_{\mathrm{B}})}{\Delta x^2}-0{\cdot}5\xi_{\mathrm{B+}}, \tag{32}$$

where subscripts B and B+ represent a point on the wall and a point adjacent to the wall respectively.

Equations (28)–(30) are modified to allow the use of the false transient method by adding the term $\alpha_\psi^{-1}\partial\phi/\partial t$ on the left-hand side of each equation, where ϕ stands for any of the variables (ξ, T or ψ). The coefficient α_ϕ has to be chosen on the basis of past experience or by trial and error.[15,16] The false transient coefficients used are the same as those used by Behnia *et al.*,[16] namely, for $Ra=10^4$: $\alpha_\psi=1$, $\alpha_\xi=0{\cdot}1$, $\alpha_T=1$ and for $Ra=10^6$: $\alpha_\phi=1$, $\alpha_\psi=0{\cdot}01$, $\alpha_T=0{\cdot}25$.

Solutions for $Ra=10^4$ and 10^6 are presented using the semi-implicit and explicit methods of internal boundary treatment (Table II). In both cases the results of the present computations agree with the benchmark solution of de Vahl Davis.[15]

Table II. Numerical efficiencies of semi-implicit (SI) and explicit (E) methods of ADI function computation at subdomain boundaries

Ra	Grid size	Number of subdomains	Stability ratio	Number of iterations	Internal boundary conditions	Damping coefficient
10^4	81×81	1	3	1554		
10^4	81×81	3×3	3	1554	SI	1
10^4	81×81	3×3	3	1689	SI	0
10^4	81×81	3×3	2	2716	E	0
10^4	81×81	3×3	1	9327	E	1
10^4	121×121	1	3	3505		
10^4	121×121	3×3	3	3514	SI	1
10^4	121×121	3×3	3	3722	SI	0
10^4	121×121	3×3	1·5	7440	E	0
10^4	121×121	3×3	1	11034	E	1
10^6	81×81	1	12	1426		
10^6	81×81	3×3	12	1511	SI	1
10^6	81×81	3×3	6	2550	SI	0
10^6	81×81	3×3	2	7615	E	0

One can see from Table II that the required number of iterations for convergence depends on the value of the stability ratio S. The maximum possible value of S depends on the chosen method of internal boundary treatment.

For the explicit method the required numbers of iterations were significantly higher than for the single-domain case. The maximal S-values for the explicit method were $S=1{\cdot}5$ for $R=0$ and $S=1$ for $R=1$. The theoretical stability analysis (see Section 4.2) for the governing equations (28)–(30) shows that for a Poisson equation ($C_x=C_y=0$) the maximal S-values are $S=2$ for $R=0$ and $S=1$ for $R=1$ (see Figure 2b). For the stability analysis for the transport equations (28) and (29) (in the frame of the approximate equality $A_x=A_y$) the C-values were computed using the maximal velocity in the cavity and the S_ϕ-values were obtained by multiplication of the value of S for the Poisson equation by the value of α_ϕ. These (S_ϕ, C) pairs are found in the stable region in the C versus S plane.

The discrepancy between the theoretical and numerical values of the maximal S for a mesh of 121×121 ($S=1{\cdot}5$ and 2 respectively) is caused by the basic assumption of the von Neumann stability analysis that ε is small (see Section 4.1). Actually for the initial iterations this assumption is not valid. Using $S=2$ at the late stages of the solution leads to convergence. This confirms our theoretical stability considerations for the case.

For the semi-implicit scheme the same S-values as in the single-domain case were utilized for stable computations (see Table II). The best numerical efficiency (measured in terms of the number of iterations) is reached for the damping coefficient $R=1$. For $Ra=10^4$ the numerical efficiency is the same as that obtained in the single-domain case. For $Ra=10^6$ (complicated flow with some recirculation regions and thin boundary layers) the observed deterioration of convergence was less than 6%.

5.3. *Turbulent duct flow*

In this case an incompressible turbulent flow field in a rectangular duct is considered. Such flows are characterized by the major axial direction of the flow. Briley[17] suggested parabolizing the Navier–Stokes equations in order to allow solution by marching in the z-direction as follows:

$$\frac{\partial F}{\partial z}=\frac{1}{ReW}\left(\frac{\partial^2 F}{\partial x^2}+\frac{\partial^2 F}{\partial y^2}\right)-\frac{U}{W}\frac{\partial F}{\partial x}-\frac{V}{W}\frac{\partial F}{\partial y}+S, \tag{33}$$

where $Re = W_0 D/\nu$ is the Reynolds number, D is the duct hydraulic diameter, W_0 is the mean inlet velocity, F represents U, V and W and S is the corresponding pressure gradient.

The streamwise pressure gradient is computed from the integral mass conservation condition[17]

$$\int_A W \mathrm{d}x\mathrm{d}y = \frac{\dot{m}}{\rho}, \tag{34}$$

where $\dot{m}$ is the mass flow rate through the duct.

The Reynolds stress model of Naot *et al.*[18] was employed. The Reynolds stress equations can be written (for this case) in the following general form

$$\frac{\partial Q}{\partial z} = \frac{1}{W}\left[\frac{\partial}{\partial x}\left(\Gamma \frac{\partial Q}{\partial x}\right) + \frac{\partial}{\partial y}\left(\Gamma \frac{\partial Q}{\partial y}\right)\right] - \frac{U}{W}\frac{\partial Q}{\partial x} - \frac{V}{W}\frac{\partial Q}{\partial y} + AQ, \tag{35}$$

where $Q = [k,\ e,\ d, \langle uw\rangle,\ \langle vw\rangle,\ \langle uv\rangle]^{\mathrm{T}}$, $k = 0{\cdot}5(u^2 + v^2 + w^2)$ is the turbulent energy, $\varepsilon = u^2 + v^2$, $d = v^2 - u^2$ and A is a rectangular matrix such that AQ represents the source terms for the Reynolds stresses (see Reference 18 for details). The apparent turbulent diffusivity is given by

$$\Gamma = C_\mu l_\mu k^{1/2}, \tag{36}$$

where C_μ is a numerical constant ($C_\mu = 0{\cdot}341$) and l_μ is the transport length scale defined as

$$l_\mu = \begin{cases} n & \text{if } 0 \leqslant n \leqslant 0{\cdot}35, \\ 0{\cdot}135 & \text{otherwise,} \end{cases} \tag{37}$$

with n being the local normal distance from the wall.

The staggered grid used enables the representation of most of the terms in the differential equations (33)–(35) by central second-order finite difference approximation.[19]

The transverse momentum equations (for U and V) are solved in two stages. In the first stage the transverse pressure gradients are approximated by their previous values and 'predicted' lateral velocities (U_{P} and V_{P}) are computed. Then a potential velocity correction is computed via a solution of a Poisson equation for the correction potential:

$$\frac{\partial^2 \phi}{\partial x^2} + \frac{\partial^2 \phi}{\partial y^2} = S, \tag{38}$$

where $S = -\nabla \vec{V}_{\mathrm{P}}$.

The Poisson equation for the potential ϕ has to be solved at every step in the z-direction. It is worthwhile noting that the equations for the Reynolds stresses (35) are different from the momentum equations owing to the presence of the coefficient matrix A. The matrix A is dense and its terms are rather large. Thus the term AQ often becomes the dominant term on the right-hand side of equations (35). A modified three-step Douglas ADI scheme[19] is utilized as follows:

$$\begin{aligned} \left(I - \frac{h_z}{2}A\right)F^* &= (A + A_x + A_y)F^n, \\ \left(I - \frac{h_z}{2}A_x\right)F^{**} &= F^*, \\ \left(I - \frac{h_z}{2}A_y\right)F^{***} &= F^*, \\ F^{n+1} &= F^n + h_z F^{***}. \end{aligned} \tag{39}$$

The solution of the first step is done by the standard Gauss elimination method for the 6×6 matrix A for each node. The second and third steps are performed using the Thomas algorithm for each line or row.

The governing fields obtained from multidomain runs on an MIMD parallel computer are the same as for single-domain computations.[19] The minimum and maximum values of the governing variables are presented in Table III, for $Re = 415{,}000$.

The stability analysis presented in Section 4 is applicable to the parabolized flow by defining ϕ_{exact} in equation (9) as the value of any of the variables U, V, W and Q in the fully developed flow or the converged solution for the Poisson equation for the potential ϕ; n is the number of the axial step or the number of the internal iteration for the Poisson equation. The parameters S and C for the momentum equations are

$$S = h_z/h_x^2 ReW, \qquad C_x = Uh_z/Wh_x, \qquad C_y = Vh_z/Wh_y. \tag{40}$$

Numerical experiments for the single-domain case and square grids suggest that the maximal value of h_z is equal to $640h_x^2$ (for example, for a grid of 81×81 points, $h_z = 0{\cdot}1$). Further increase in h_z leads to divergence owing to the non-linearity of the problem.

Using the values from Table III, it is possible to calculate S and C by (40) as functions of the axial velocity W (where $W_{\max} \leqslant W \leqslant W_{\min}$). The values of C_{crit} (corresponding to $U_{\max}$ and $U_{\min}$) versus S are shown in Figure 7 (segments A_1B_1 and A_2B_2). For the case considered, these values of C_{crit} versus S are inside the stability region for the explicit scheme of internal boundary treatment. Thus one can use the explicit scheme for multidomain solution of the momentum equations.

For the Reynolds stress equations the value of S is determined by

$$S = h_z\Gamma/h_x^2 W, \tag{41}$$

where Γ is computed by (36). An estimate of Γ shows that $S > 2$. Owing to the recirculatory nature of the problem, there are internal boundaries with negative values of U or V. It was already pointed out that the explicit scheme is unstable for $S > 2$ and negative C-values. An attempt to use the explicit scheme for the Reynolds stress equations actually led to divergence. Thus the semi-implicit scheme is required for the Reynolds stress equations.

For the Poisson equation the Courant number C is zero and $S = h_t/h_x^2$. Numerical experiments for the single-domain case have shown that $h_t = 1{\cdot}3h_x^2$ yields the minimal number of iterations for the Poisson equation. The maximal value of the damping coefficient R ensuring that the explicit scheme for the internal boundaries is still stable was found to be $R = 0{\cdot}25$ and was utilized in the multidomain parallel computations.

Some results of parallel computer runs are presented in Table IV for a 200×200 grid for runs on a MEIKO parallel computer. More detailed results of the parallel computations are given in Reference 2.

The reason for 'over speed-up' for the 2×2 partitioning is that the solution of the Poisson equation requires many more iterations in the single-domain case than in the parallel case. This is probably caused by round-off errors due to the application of the Thomas algorithm to large matrices.

Table III. Minimum and maximum values of governing variables

	W	$U \times 10^2$	$V \times 10^2$	$k \times 10^2$	$e \times 10^2$	$d \times 10^2$	$\langle uw \rangle \times 10^2$	$\langle uv \rangle \times 10^3$
Max.	1·155	1·629	1·629	1·481	0·839	0·297	0·292	0·106
Min.	0·584	−1·629	−1·629	0·559	0·424	−0·297	−0·292	−0·106

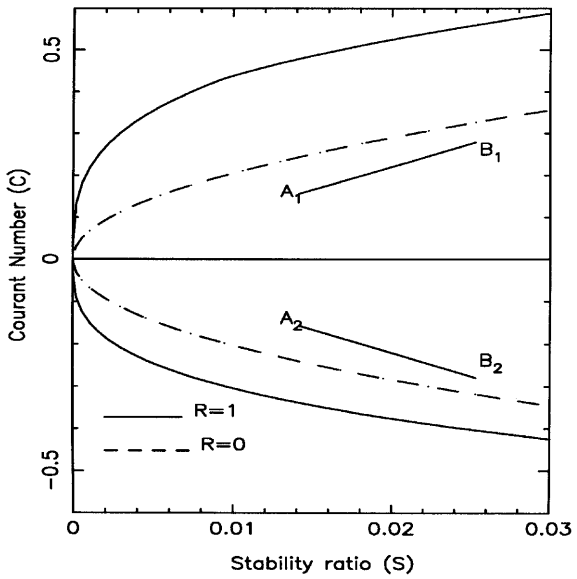

Figure 7. Stability region of momentum equations for turbulent duct flow. Segments A_1B_1 and A_2B_2 show C versus S

Table IV. Computation times for 200×200 grid and various partitionings of square duct

Partitioning	Elapsed time (h)	Speed-up
Serial	104·0	–
2×2	19·2	5·4
3×3	12·1	8·6
4×4	13·8	7·5

5. CONCLUSIONS

A multidomain method for the solution of elliptic CFD problems with an ADI scheme is described. An advantage of the method is that calculations in each subdomain must wait for their neigbours only and need not wait for completion of each step of the solution. Two methods of treatment of internal boundary conditions for ADI functions are proposed, namely an explicit and a semi-implicit methods. A theoretical method for determining the stability conditions (in terms of the stability ratio S and the Courant number C) is developed and confirmed by computations for various test cases.

The stability region of the semi-implicit scheme is significantly broader than that of the explicit scheme because: (i) the stability condition is symmetrical for positive and negative Courant number values; (ii) the region of stability is sufficiently larger; (iii) for zero damping coefficient ($R = 0$) and for the stability number $S \rightarrow \infty$ the scheme is stable for $|C/S| \leqslant 2$; (iv) for $S \rightarrow 0$ the scheme is stable for $|C| \leqslant C_{\text{crit}}$.

It is shown that using the semi-implicit scheme makes it possible to utilize the same values of S as in the single-domain computations. The number of iterations of the semi-implicit method is close to that required in a single-domain computation.

APPENDIX I: ASYMPTOTIC INVESTIGATION OF STABILITY FOR EXPLICIT SCHEME

The purpose of this appendix is to obtain analytically the stability region for large S. It is proven that for zero damping coefficient ($R=0$) the stability region approaches the line $C_x/S_x=2$. For the common case ($R\neq 0$) it is shown that the scheme is stable for $C_x/S_x=2$ and $C_y/S_y=2$. (We do not prove that the above limiting values are singular. However, the numerical computations of the amplification factor for the explicit scheme (see Section 4.2) have not shown another stability region for large S.)

Firstly we consider the asymptotic behaviour ($S\to\infty$) of the stability region for the particular case where the damping coefficient vanishes ($R=0$). In this case the coefficient C (equation (20)) is zero and the quadratic equation (19) for the amplification factor G becomes linear, yielding

$$G=1-\frac{X+Y}{\left(1+\frac{Y}{2}\right)\left[1+S_x-\left(\frac{S_x}{2}+\frac{C_x}{4}\right)\mathrm{e}^{-\theta_x \mathrm{i}}\right]}. \tag{42}$$

When $A_y=0$, the above expression for G becomes

$$\begin{aligned} G_x &= 1-\frac{X}{1+S_x-\left(\frac{S_x}{2}+\frac{C_x}{4}\right)\mathrm{e}^{-\theta_x \mathrm{i}}} \\ &= \frac{\frac{1}{S_x}-1-\left(\frac{1}{2}+\frac{Re}{4}\right)\mathrm{e}^{-\theta_x \mathrm{i}}+2\cos(\theta_x)-Re\sin(\theta_x)\mathrm{i}}{\frac{1}{S_x}+1-\left(\frac{1}{2}+\frac{Re}{4}\right)\mathrm{e}^{-\theta_x \mathrm{i}}} \end{aligned} \tag{43}$$

where $Re=C_x/S_x$ is the cell Reynolds number and G_x is the amplification factor for the particular case $A_y=0$.

Neglecting the terms $1/S_x$ for large S_x and utilizing the condition of stability $|G|\leqslant 1$/* the following inequality is obtained for the cell Reynolds number Re:

$$Re^2\sin^2(\theta_x)-2Re[1-\cos(\theta_x)]-4\cos(\theta_x)[1-\cos(\theta_x)]\leqslant 0, \tag{44}$$

where $0<\theta_x<2\pi$. For a given value of θ_x the roots of inequality (44) are 2 and $-2\cos(\theta_x)/[1+\cos(\theta_x]$. For $\cos(\theta_x)=-\frac{1}{2}$ the roots are equal and a single value ($Re=2$) satisfies inequality (44).

For the case $A_y\neq 0$ we multiply both sides of (42) by $1+Y/2$:

$$G\left(1+\frac{Y}{2}\right)=G_x+\frac{Y}{2}\left(1-\frac{2}{1+S_x-\left(\frac{S_x}{2}+\frac{C_x}{4}\right)\mathrm{e}^{-\theta_x \mathrm{i}}}\right). \tag{45}$$

where G_x was obtained by (43). In this equation the last term vanishes for large S_x. Therefore the expression in large parentheses tends to unity.

The asymptotic expression for G in the case of large S_x is given by

$$(Y/s)(G-1)+G=G_x. \tag{46}$$

*The absolute value of a complex number $G=(a+b_\mathrm{i})/(c+d_\mathrm{i})$ is computed by $|G|=|a+b_\mathrm{i}|/|c+d_\mathrm{i}|=\sqrt{[(a^2+b^2)/(c^2+d^2)]}$.

The right-hand side of the above equation does not depend on θ_y. Therefore the left-hand side cannot depend on θ_y either. For the specific value $\theta_y \approx 0$, Y is close to zero and thus $G \approx G_x$ for large S_x. It was shown above that $|G_x| \leqslant 1$ for $S_x/C_x = 2$.

For the common case ($R \neq 0$) the cell Reynolds number $Re = 2$ satisfies the stability condition for large S_x. Actually for $Re = 2$ the terms $R(C_x/4 - S_x/2)e^{\theta_x i}$ in expressions (20) vanish. Therefore the expression for the amplification factor is exactly the same as (42) and all previous considerations are valid.

For corner points (boundary points belonging to both the X- and Y internal boundaries) the left-hand side of equation (14) would be replaced by an analogue of expression (18) for the Y-direction. The quadratic equation for the amplification factor G has the coefficients

$$\begin{aligned} A &= \left[1 + S_y - \left(\frac{S_y}{2} + \frac{C_y}{4}\right)e^{-\theta_y i}\right]\left[1 + S_x - \left(\frac{S_x}{2} + \frac{C_x}{4}\right)e^{-\theta_x i}\right], \\ C &= -R\left\{\left(\frac{C_x}{4} - \frac{S_x}{2}\right)e^{\theta_x i} + \left(\frac{C_y}{4} - \frac{S_y}{2}\right)e^{\theta_y i}\left[1 + S_x - \left(\frac{S_x}{2} + \frac{C_x}{4}\right)e^{-\theta_x i}\right]\right\}, \\ B &= X + Y - (A + C). \end{aligned} \tag{47}$$

The asymptotic stability of a corner point is the same as for a regular boundary point. Under the condition $C_x/S_x = C_y/S_y = 2$ the terms $R(C_x/4 - S_x/2)e^{\theta_x i}$ and $R(C_y/4 - S_y/2)e^{\theta_y i}$ in the above expressions vanish and $C = 0$. The expression for G has a very similar pattern to that for a regular boundary point, except that the term $1 + Y/2$ is replaced by $1 + S_y - (S_y/2 + C_y/4)e^{-\theta_y i}$. However, for $C_y/S_y = 2$ these terms are equal. Therefore for $S_y \to \infty$ the proposed scheme is stable at corner points under the same condition $C_x/S_x = C_y/S_y = 2$ as at regular boundary points.

APPENDIX II: ASYMPTOTIC INVESTIGATION OF STABILITY FOR SEMI-IMPLICIT SCHEME

We shall prove that for large S and zero damping coefficient ($R = 0$) the numerical scheme is stable if $|Re| \leqslant 2$. For $R > 0$ we show that the scheme is stable if $|Re| = 0$ or 2.

We prove that for small S and $R = 0$ the scheme is stable if $|Re| \leqslant 4$.

For the case $R = 0$ the coefficient C from (25) is equal to zero and the quadratic equation (19) becomes linear. The expression for the amplification factor G has the form

$$G = 1 - \frac{(X + Y)(1 + S_x)}{\left(1 + \frac{Y}{2}\right)\left[1 + S_x - \left(\frac{S_x}{2} + \frac{C_x}{4}\right)e^{-\theta_x i}\right]\left[1 + S_x - \left(\frac{S_x}{2} - \frac{C_x}{4}\right)e^{\theta_x i}\right]}. \tag{48}$$

When $A_y = 0$, expression (48) becomes

$$G = \frac{\left[\frac{1}{S_x} + 1 - \left(\frac{1}{2} + \frac{Re}{4}\right)e^{-\theta_x i}\right]\left[\frac{1}{S_x} + 1 - \left(\frac{1}{2} - \frac{Re}{4}\right)e^{\theta_x i}\right] - 2[1 - \cos(\theta_x)] - Re\,\sin(\theta_x)\left(\frac{1}{S_x} + 1\right)i}{\left[\frac{1}{S_x} + 1 - \left(\frac{1}{2} + \frac{Re}{4}\right)e^{-\theta_x i}\right]\left[\frac{1}{S_x} + 1 - \left(\frac{1}{2} - \frac{Re}{4}\right)e^{\theta_x i}\right]}. \tag{49}$$

For large S_x the terms $1/S_x$ are negligible, so

$$G = \frac{-\frac{3}{4} - \left(\frac{Re}{4}\right)^2 + \cos(\theta_x) - \frac{Re}{2}\sin(\theta_x)\mathrm{i}}{\frac{5}{4} - \left(\frac{Re}{4}\right)^2 - \cos(\theta_x) + \frac{Re}{2}\sin(\theta_x)\mathrm{i}}. \tag{50}$$

The stability condition $|G| < 1$ leads to the inequality

$$\left[\left(\frac{Re}{2}\right)^2 - 1\right][1 - \cos(\theta_x)] \leqslant 0, \tag{51}$$

which is satisfied when

$$-2 \leqslant Re \leqslant 2. \tag{52}$$

For the case $R > 0$ and $|Re| = 2$ the coefficient C in (25) is equal to zero. Therefore expression (48) for the amplification factor is valid and according to condition (52) the scheme is stable.

For the case $|Re| = 0$ the coefficients (25) of the quadratic equation (19) become

$$A = (1 + S_x)^2 - \left(\frac{S_x}{2}\right)^2, \qquad C = R\left(\frac{S_x}{2}\right)^2, \qquad B = X - (A + C), \tag{53}$$

where $X = 4S_x \sin^2(\theta_x/2)$.

Only the terms S_x^2 are taken into consideration in (53) and the above coefficients are given by

$$A = \frac{3}{4}\left(\frac{S_x}{2}\right)^2, \qquad C = R\left(\frac{S_x}{2}\right)^2, \qquad B = -(A + C). \tag{54}$$

The roots of equation (19) for the amplification factor are -1 and $R/3$. For refinement of the analysis, S_x is taken into account in (53). The coefficients A and C are the same as in (54) and the coefficient B becomes $B = X - (A + C)$, where $X > 0$ for $\theta_x > 0$. Therefore the amplication factor is bigger than -1 and the scheme is stable for every finite S_x.

The proof that the above asymptotic conditions are valid for the common case $A_y \neq 0$ is performed in the same way as for the explicit scheme.

When $R = 0$ and $A_y = 0$, the stability condition is obtained analytically for small S_x-values, when $S_x^2 \ll S_x$, and (48) becomes

$$G = \frac{1 - \left(\frac{C_x}{4}\right)^2 + S_x\cos(\theta) - \frac{C_x}{2}\sin(\theta)\left(1 + \frac{S_x}{2}\right)\mathrm{i}}{1 - \left(\frac{C_x}{4}\right)^2 - S_x\cos(\theta) + 2S_x + \frac{C_x}{2}\sin(\theta\left(1 + \frac{S_x}{2}\right)\mathrm{i}}. \tag{55}$$

The stability condition $|G|1$ leads to the following inequality for C_x:

$$\left[1 - \left(\frac{C_x}{4}\right)^2\right]2S_x\cos(\theta) \leqslant \left[1 - \left(\frac{C_x}{4}\right)^2\right]2S_x[2 - \cos(\theta)]. \tag{56}$$

The resulting restriction for the Courant number C_x is

$$-4 \leqslant C_x \leqslant 4. \tag{57}$$

APPENDIX III: LIST OF MAIN SYMBOLS

A_x, A_y	differential operators in x- and y-direction respectively
$C_x = U\delta t/\Delta x$	Courant number in x-direction
$C_y = V\Delta t/\Delta y$	Courant number in y-direction
f^*, f^{**}	intermediate ADI functions
F, ϕ	main variables
G	amplification factor for error
P, Q	amplification factors for f^*, f^{**}
Pr	Prandtl number
R	damping coefficient
Ra	Rayleigh number
S	source term
$S_x = v\Delta t/\Delta x^2$	stability ratio in x-direction
$S_y = v\Delta t/\Delta x^2$	stability ratio in y-direction
U, V	velocity components in x- and y-direction respectively

Greek letters

ε	error (difference between exact and numerical solutions)
θ_x, θ_y	phase angles
ξ	vorticity
ψ	streamfunction

REFERENCES

1. R. Hackney, *Parallel Computers*, 2nd edn, Hilger, Bristol, 1988.
2. A. Povitsky and M. Wolfshtein, 'Numerical solution of flow problems on a parallel computer', *AIAA Paper 95-1697*, 1995.
3. N. H. Naik, V. K. Naik and M. Nicoules, 'Parallelization of a class of implicit finite difference schemes in computational fluid dynamics', *Int. J. High Speed Comput.* **5**, 1–50 (1993).
4. M. Rosenfeld and Y. Yassour, 'The alternating direction multi-zone implicit method', *J. Comput. Phys.* **110**, 212–220 (1994).
5. E. Schreck and M. Peric, 'Computation of fluid flow with a parallel multi-grid solver', *Int. j. numer. methods fluids*, **16**, 303–327 (1993).
6. M. C. Tsai, 'Parallel algorithm for simulating Marangoni convection in a three dimensional cavity', *ASME Paper 93-WA/HT-68*, 1993.
7. M. Braten, 'Solution of viscous fluid flows on a distributed memory concurrent computer', *Int. j. numer. methods fluids*, **10**, 889–905 (1990).
8. C. B. Jenssen, 'Implicit multiblock Euler and Navier–Stokes calculations', *AIAA J.* **32**, 1808–1814 (1994).
9. D. Degani and S. Marcus, 'Implementation obstacles of domain decomposition schemes', *AIAA Paper 95-0569*, 1995.
10. T. L. Tysinger and D. A. Caughey, 'Distributed parallel processing applied to an implicit multigrid Euler/Navier–Stokes algorithm', *AIAA Paper 93-0057*, 1993.
11. J. Isenberg and G. de Vahl Davis. *Finite Difference Methods in Heat and Mass Transfer*, Technion, Haifa, 1974.
12. C. A. J. Fletcher, *Computational Techniques for Fluid Mechanics*, Springer, Berlin, 1988.
13. J. Trapp and J. Ramshaw, 'A simple heuristic method for analyzing the effect of boundary conditions on numerical stability', *J. Comput. Phys.*, **20**, 238–242 (1976).
14. P. Roache, *Computational Fluid Dynamics*, Hermosa, Albuqerque, NM, 1976.
15. G. de Vahl Davis, 'Natural convection of air in a square cavity: a bench mark numerical solution', *Int. j numer. methods fluids*, **3**, 249–264 (1983).
16. M. Behnia, M. Wolfshtein and G. de Vahl Davis, 'A stable fast marching scheme for computational fluid mechanics', *Int. j numer. methods fluids*, **10**, 607–621 (1990).
17. W. R. Briley. 'Numerical method for predicting three-dimensional steady viscous flow in ducts', *J. Comput. Phys.* **14**, 8–28 (1974).
18. D. Naot, A. Shavit and M. Wolfshtein, 'Numerical calculations of Reynolds stresses in a square duct with secondary flow', *Warme- und Stoffubertragung*, **7**, 151–161 (1974).

